ChemInform Abstract: Dynamic Distribution of Growth Rates within the Ensembles of Colloidal II–VI and III–V Semiconductor Nanocrystals as a Factor Governing Their Photoluminescence…

ARTICLE *in* JOURNAL OF THE AMERICAN CHEMICAL SOCIETY · JUNE 2002

Impact Factor: 12.11 · DOI: 10.1021/ja0123599 · Source: PubMed

6 AUTHORS, INCLUDING:

Dmitri V Talapin
University of Chicago
160 PUBLICATIONS **16,259** CITATIONS
SEE PROFILE

Elena V Shevchenko
Argonne National Laboratory
90 PUBLICATIONS **9,342** CITATIONS
SEE PROFILE

Horst Weller
University of Hamburg
390 PUBLICATIONS **26,842** CITATIONS
SEE PROFILE

J|A|C|S
ARTICLES
Published on Web 04/30/2002

Dynamic Distribution of Growth Rates within the Ensembles of Colloidal II−VI and III−V Semiconductor Nanocrystals as a Factor Governing Their Photoluminescence Efficiency

Dmitri V. Talapin,*,† Andrey L. Rogach,† Elena V. Shevchenko, Andreas Kornowski, Markus Haase, and Horst Weller

Contribution from the Institute of Physical Chemistry, University of Hamburg, 20146 Hamburg, Germany

Received October 15, 2001

Abstract: The distribution of properties within ensembles of colloidally grown II−VI and III−V semiconductor nanocrystals was studied. A drastic difference in the photoluminescence efficiencies of size-selected fractions was observed for both organometallically prepared CdSe and InAs colloids and for CdTe nanocrystals synthesized in aqueous medium, indicating a general character of the phenomenon observed. The difference in the photoluminescence efficiencies is attributed to different averaged surface disorder of the nanocrystals originating from the Ostwald ripening growth mechanism when larger particles in the ensemble grow at the expense of dissolving smaller particles. At any stage of growth, only a fraction of particles within the ensemble of growing colloidal nanocrystals has the most perfect surface and, thus, shows the most efficient photoluminescence. This is explained by a theoretical model describing the evolution of an ensemble of nanocrystals in a colloidal solution. In an ensemble of growing nanocrystals, the fraction of particles with the highest photoluminescence corresponds to the particle size having nearly zero average growth rate. The small average growth rate leads to the lowest possible degree of surface disorder at any given reaction conditions.

Introduction

A number of synthetic routes to highly crystalline nearly monodisperse II−VI[1−7] and III−V[8−12] semiconductor nanoparticles were developed during the last years. Some of them yield nanocrystals with high and stable photoluminescence (PL), making them suitable for optoelectronic[13−16] and tagging[17−19] applications. On the other hand, only a few general aspects of the growth kinetics of colloidal nanocrystals were described.[20−23] Since nanocrystals lie in the transition region between molecular species and bulk materials, their growth kinetics can be discussed using either molecular[24] or solid-state[25] terminology. The structure of the nanocrystal surface at any given instant of time has to depend, for instance, on the rates at which matter joins the surface or leaves it and on the mobility of the surface atoms. However, the stabilizing shell always present at the surface of colloidal nanocrystals affects all these processes and makes difficult any attempt of direct probing of nanocrystal surface. Moreover, the properties of nanocrystals in colloidal solution are always averaged over the whole ensemble and can differ from those of a single particle. As an example, photoluminescence blinking can be observed only for a single nanocrystal, but never for an ensemble.[26]

* Author to whom correspondence should be addressed. Fax: +49-40-42838-3452. E-mail: talapin@chemie.uni-hamburg.de. Web site: http://www.chemie.uni-hamburg.de/pc/AKs/Weller/

† On leave from the Physico-Chemical Research Institute, Belarusian State University, Minsk, Belarus.

(1) Murray, C. B.; Norris, D. J.; Bawendi, M. G. *J. Am. Chem. Soc.* **1993**, *115*, 8706.
(2) Vossmeyer, T.; Katsikas, L.; Giersig, M.; Popovic, I. G.; Diesner, K.; Chemseddine, A.; Eychmüller, A.; Weller, H. *J. Phys. Chem.* **1994**, *98*, 7665.
(3) Peng, Z. A.; Peng, X. *J. Am. Chem. Soc.* **2001**, *123*, 183.
(4) Talapin, D. V.; Rogach, A. L.; Kornowski, A.; Haase, M.; Weller, H. *Nano Lett.* **2001**, *1*, 207.
(5) Dabbousi, B. O.; Rodriguez-Viejo, J.; Mikulec, F. V.; Heine, J. R.; Mattoussi, H.; Ober, R.; Jensen, K. F.; Bawendi, M. *J. Phys. Chem. B* **1997**, *101*, 9463.
(6) Peng, X.; Schlamp, M. C.; Kadavanich, A.; Alivisatos, A. P. *J. Am. Chem. Soc.* **1997**, *119*, 7019.
(7) Talapin, D. V.; Haubold, S.; Rogach, A. L.; Kornowski, A.; Haase, M.; Weller, H. *J. Phys. Chem. B* **2001**, *105*, 2260.
(8) Micic, O. L.; Curtis, C. J.; Jones, K. M.; Sprague, J. R.; Nozik, A. J. *J. Phys. Chem.* **1994**, *98*, 4966.
(9) Guzelian, A. A.; Katari, J. E. B.; Kadavanich, A. V.; Banin, U.; Hamad, K.; Juban, E.; Alivisatos, A. P.; Wolters, R. H.; Arnold, C. C.; Heath, J. R. *J. Phys. Chem.* **1996**, *100*, 7212.
(10) Guzelian, A. A.; Banin, U.; Kadavanich, A. V.; Peng, X.; Alivisatos, A. P. *Appl. Phys. Lett.* **1996**, *69*, 1432.
(11) Cao, Y. W.; Banin, U. *J. Am. Chem. Soc.* **2000**, *122*, 9692.
(12) Cao, Y. W.; Banin, U. *Angew. Chem., Int. Ed.* **1999**, *38*, 3692.
(13) Colvin, V. L.; Schlamp, M. C.; Alivisatos, A. P. *Nature* **1994**, *370*, 354.
(14) Schlamp, M. C.; Peng, X.; Alivisatos, A. P. *J. Appl. Phys.* **1997**, *82*, 5837.
(15) Gao, M.; Lesser, C.; Kirstein, S.; Möhwald, H.; Rogach, A. L.; Weller, H. *J. Appl. Phys.* **2000**, *87*, 2297.
(16) Klein, D. L.; Roth, R.; Lim, A. K. L.; Alivisatos, A. P.; McEuen, P. L. *Nature* **1997**, *389*, 699.
(17) Bruchez, M. P.; Moronne, M.; Gin, P.; Weiss, S.; Alivisatos, A. P. *Science* **1998**, *281*, 2013.
(18) Chan, W. C. W.; Nie, S. *Science* **1998**, *281*, 2016.
(19) Han, M.; Gao, X.; Su, J. Z.; Nie, S. *Nat. Biotechnol.* **2001**, *19*, 631.
(20) Peng, X.; Wickham, J.; Alivisatos, A. P. *J. Am. Chem. Soc.* **1998**, *120*, 5343.
(21) Peng, Z. A.; Peng, X. *J. Am. Chem. Soc.* **2001**, *123*, 1389.
(22) Peng, X.; Manna, L.; Yang, W.; Wickham, J.; Scher, E.; Kadavanich, A.; Alivisatos, A. P. *Nature* **2000**, *404*, 59.
(23) Talapin, D. V.; Rogach, A. L.; Haase, M.; Weller, H. *J. Phys. Chem. B* **2001**, *105*, 12278.
(24) Steigerwald, M. L.; Brus, L. E. *Acc. Chem. Res.*, **1990**, *23*, 183.
(25) Jackson, K. A. *J. Cryst. Growth* **1999**, *198/199*, 1.

10.1021/ja0123599 CCC: $22.00

The intrinsic polydispersity of particles in colloidal solution usually results in the Ostwald ripening growth mechanism, where smaller particles dissolve, providing the monomers for building the large ones.[27] Peng et al.[20] showed experimentally that the growth of nanocrystals in colloidal solutions occurs either with a "focusing" of size distribution if the monomer concentration in the solution is high and all the nanocrystals grow with narrowing of the size distribution or through Ostwald ripening, when the larger particles grow at the expense of smaller particles, resulting in broadening of the size distribution. Peng also showed that this behavior is in accord with the model of Sugimoto.[28] "Focusing" and "defocusing" of size distribution do not originate from different particle growth mechanisms and can be described in the framework of the same kinetic model of evolution of an ensemble of nanoparticles in a colloidal solution.[23] Here and below, we use the term "ensemble" to describe the whole population of particles present in the colloidal solution at different instants of time. Following Peng,[21] we use the term "monomer" to describe any molecular species, excluding nanocrystals, containing Cd, In, As, Se, or Te, which are necessary for the formation and growth of nanocrystals. During Ostwald ripening, the particles in an ensemble have different growth rates,[23] which has to affect their properties to some extent. Thus, larger particles have positive growth rates while smaller particles show negative ones. To investigate the variation of properties with the particle size, the ensemble of nanocrystals can be further divided into nearly monodisperse fractions by applying a so-called size-selective precipitation procedure.[1,29]

To the best of our knowledge, there were no thorough studies on the distribution of properties within an ensemble of growing nanocrystals. In this paper, we have investigated how the particle properties do vary within the colloidally grown ensembles of CdSe, CdTe, and InAs nanocrystals.

Experimental Section

Synthesis of CdSe, CdTe, and InAs Nanocrystals. To explore the general behavior of semiconductor nanocrystals, we tested II−VI and III−V colloids, both prepared via well-established synthetic routes.

CdSe nanocrystals were prepared by a high-temperature organometallic synthesis following Murray et al.[1] One millimole of TOPSe[30] and 1.35 mmol of dimethylcadmium were dissolved in 5 mL of trioctylphosphine (TOP) and rapidly injected into a vigorously stirred 10 g of trioctylphosphine oxide (TOPO) heated to 360 °C. Further growth occurred at 300 °C for different periods of time, depending on the desired size of the CdSe nanocrystals.

Aqueous colloids of CdTe nanocrystals capped by thioglycolic acid (TGA) were synthesized as reported in refs 31 and 32 with the difference that H_2Te gas was used as the tellurium source instead of NaHTe solution. Briefly, 500 mL of a solution containing 0.013 M $Cd(ClO_4)_2$ and 0.02 M TGA was adjusted to pH 11.2 by addition of a 1 M solution of NaOH. Then H_2Te gas obtained by the decomposition of 0.8 g of Al_2Te_3 with an excess of 0.05 M H_2SO_4 was passed in a nitrogen flow at room temperature into this solution. The CdTe precursors formed thereby were converted into CdTe nanocrystals by refluxing the solution at 100 °C. Portions of CdTe nanocrystals of different sizes were taken from the crude solution at different refluxing times. The TGA capping of CdTe nanocrystals makes them air-stable and processable at ambient conditions. Thus, aqueous colloids of CdTe nanocrystals showed no changes in optical properties during months of storage in air.

InAs nanocrystals were synthesized by the dehalosilylation reaction[10,11] between $InCl_3$ and tris(trimethylsilyl)arsine (TMS_3As). In a typical preparation route, 0.30 g of $InCl_3$ was dissolved in 1 mL of TOP, mixed with 0.26 mL of TMS_3As, and rapidly injected into 3.2 g of TOP vigorously stirred at 300 °C. Further growth occurred at 260 °C for different periods of time depending on the desired size of the nanocrystals. To keep the particle size distribution narrow and to prepare InAs particles larger than ∼3.5 nm in size, additional injections of precursors were necessary.

Size-Selective Precipitation of Nanocrystals. As the conclusions drawn in this work were based on investigations of size-selectively isolated fractions of nanocrystals, we paid special attention to all procedures involving their postpreparative treatment. First, all manipulations with organometalically prepared CdSe and InAs nanocrystals were performed inside a glovebox under nitrogen atmosphere. Second, we carried out control experiments for all nanocrystals investigated to ensure that no changes of properties were induced by size-selective precipitation.

Size-selective precipitation of aqueous CdTe colloids was carried out as follows. Aliquots of the crude solution were concentrated by a factor of ∼3 in a rotor evaporator at 25−40 °C, and 2-propanol was added dropwize under stirring until the solution become slightly turbid. The precipitate was isolated by centrifugation and redissolved in the defined volume of water. The procedure was repeated several times allowing us to obtain 6−12 size-selected fractions of CdTe nanocrystals from each portion of the crude solution.

In the case of CdSe and InAs nanocrystals, the TOPO−TOP stabilizing shell is, probably, more labile as compared to the TGA shell on CdTe nanocrystals and can be partially washed out if the concentration of TOP in the solution is low. As a result, a systematic decrease of the PL efficiency of size-selected fractions in comparison with the initial crude solutions was observed. To overcome this problem, we carried out the size-selective precipitation under an inert gas atmosphere and the concentration of TOP was kept at a constant value. Aliquots of the crude solution of either CdSe or InAs nanocrystals were taken from the hot reaction mixture, cooled to room temperature, and mixed with a ∼10-fold excess of 1-butanol (in the case of CdSe) or toluene (in the case of InAs). Methanol or ethanol was added dropwize until the solutions became turbid, and the precipitates were isolated by filtration through 0.2-μm PTFE filters. Subsequently, TOP was added to the supernatant to keep the concentration of TOP at one constant level (5−10 wt %) at all stages of size-selective precipitation. For optical measurements, the precipitate was redissolved in a 10 vol % solution of TOP in toluene. This procedure was repeated 8−12 times to obtain a series of size-selected fractions of nanocrystals. Unfortunately, toluene has strong absorption bands around 1 eV that disturb the PL spectra of InAs nanocrystals larger than ∼3.5 nm. The use of solvents transparent in the near-IR, e.g., CCl_4, did not allow us to prepare InAs colloids that were stable for long periods of time. Therefore, we worked only with colloids of relatively small InAs nanocrystals emitting above 1 eV. To achieve quantitative reproducibility of the optical measurements, the solutions of nanocrystals were removed from the glovebox only in sealed quartz cuvettes, preventing any contact of organometallically prepared colloids with air.

Apparatus. UV−visible absorption spectra were taken on a Cary 500 (Varian) spectrophotometer. PL spectra in the visible (CdSe, CdTe) and near-IR (InAs) spectral regions were measured, respectively, with a Fluoromax-2 (Instruments SA) spectrofluorometer and a custom-made spectrofluorometer with a nitrogen-cooled germanium detector and lock-in amplification. The latter was thoroughly calibrated using the known

(26) Empedocles, E. A.; Neuhauser, R.; Shimizu, K.; Bawendi, M. G. *Adv. Mater*. **1999**, *11*, 1243.
(27) Ostwald, W. *Z. Phys. Chem*. **1901**, *37*, 385.
(28) Sugimoto, T. *Adv. Colloid Interface Sci.* **1987**, *28*, 65.
(29) Chemseddine, A.; Weller, H. *Ber. Bunsen-Ges. Phys. Chem.* **1993**, *97*, 636.
(30) Preparation of TOPSe is described in ref 1.
(31) Rogach, A. L.; Katsikas, L.; Kornowski, A.; Su, D.; Eychmüller, A.; Weller, H. *Ber. Bunsen-Ges. Phys. Chem.* **1996**, *100*, 1772.
(32) Gao, M.; Kirstein, S.; Möhwald, H.; Rogach, A. L.; Kornowski, A.; Eychmüller, A.; Weller, H. *J. Phys. Chem. B* **1998**, *102*, 8360.

spectrum of a tungsten−halogen lamp as reported by Cao and Banin.[11] All PL spectra of colloidal solutions were measured at optical densities at the excitation wavelength between 0.10 and 0.14. The small values of optical density guaranty that no artifacts can arise from different light penetration depths. The photoluminescence excitation spectra were found to be nearly identical to the absorption spectra in a wide spectral region for all samples studied. The latter indicates no dependence of the emission spectra on the excitation wavelength. If not specially mentioned in text, excitation wavelengths of 400 nm were used for CdSe and CdTe nanocrystals and of 600 nm for InAs nanocrystals. To compare the PL efficiencies of different samples, we normalized each PL spectrum with respect to the absorbed light intensity at the excitation wavelength and subsequently integrated the PL intensity versus photon energy over the entire emission spectrum. The absolute values of room-temperature PL efficiency of nanocrystals were estimated by comparison with solutions of Rhodamine 6G in ethanol (CdSe), quinine in aqueous 0.5 M H_2SO_4 (CdTe), and IR 125 dye (Lambda Physik) in DMSO (InAs). We used literature values for the room-temperature PL efficiencies of these dyes, i.e., 0.95,[33] 0.55,[34] and 0.13,[11] respectively.

Powder X-ray diffraction spectra were taken on a Philips X′Pert diffractometer (Cu Kα radiation, variable entrance slit, Bragg−Brentano geometry, secondary monochromator). High-resolution transmission electron microscopy (HRTEM) and energy-dispersive X-ray analysis (EDX) were performed on a Phillips CM-300 microscope operating at 300 kV. TEM samples were prepared by dropping dilute solutions of nanocrystals onto 400-mesh carbon-coated copper grids and immediately evaporating the solvent.

To investigate the photostability of nanocrystals, dilute colloidal solutions (either saturated with oxygen or under air-free conditions) were excited at $\lambda_{ex} = 400$ nm for different intervals of time using a 450-W xenon lamp and a band-pass interference filter (K40 Balzers).

Results

1. Growth of CdSe, CdTe, and InAs Nanocrystals in Crude Solutions. The synthesis of nanocrystals involves stages of nucleation and growth that may either take place separately or partially overlap in time. The former case is realized when the so-called "hot injection" technique[1] is applied, where the precursors are rapidly injected into a hot coordinating solvent resulting in very fast nucleation followed by subsequent growth of the nuclei at lower temperature. During the growth stage, a large number of colloidal particles compete for a finite amount of monomer, and the total number of particles decreases slowly due to dissolution of the small ones. The strong size dependence of the optical properties of semiconductor nanocrystals allows one to monitor the mean particle size and the size distributions through the temporal evolution of UV−visible and PL spectra.[2,20]

Figure 1 shows absorption and PL spectra of crude CdSe, CdTe, and InAs colloidal solutions taken from the reaction flasks at different stages of particle growth. Both the absorption and the PL spectra of the nanocrystals shifted to longer wavelengths as the particle size increased as a consequence of the quantum confinement effect. The width of the absorption and PL bands reflects the size distributions of the nanocrystals in the crude solutions. In the case of CdSe and InAs nanocrystals grown by the hot injection technique, two regimes of particle growth were observed. During the first ∼30 min, the size distribution narrowed (focusing) and then started to broaden (defocusing). This behavior observed by Peng et al. was attributed to different

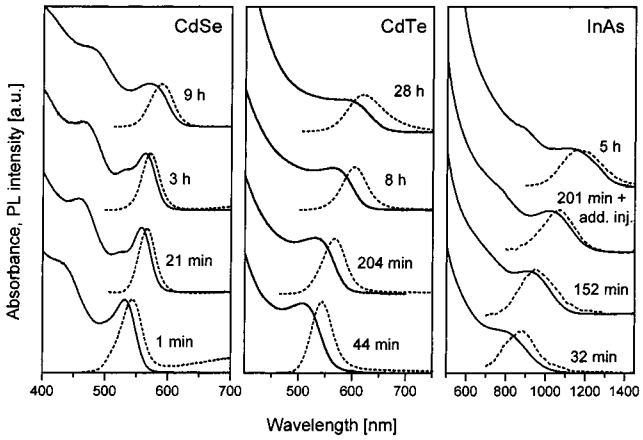

Figure 1. Temporal evolution of absorption (solid lines) and PL (dashed lines) spectra of CdSe, CdTe, and InAs nanocrystals during their growth in crude solutions. The widths of the PL bands reflect the intrinsic particle size distributions in the crude solution at different stages of growth. In the case of InAs nanocrystals, additional precursor was injected into the reaction mixture to keep size distribution narrow (marked as "add. inj.").

particle growth modes.[20] During the focusing stage, all nanocrystals grow via reaction with the excess of monomer present in the solution after nucleation. During the defocusing stage, nanocrystals grow via Ostwald ripening accompanied by gradual decrease of the particle concentration. During the growth of CdTe nanocrystals in aqueous solution, no focusing of particle size distribution was observed. Nevertheless, rather narrow PL spectra of CdTe nanocrystals (fwhm 45−55 nm) corresponding to ∼15% particle size distribution observed at initial stages of the synthesis evidenced that the nucleation and the particle growth stages were rather well separated in time even without applying the hot injection technique. This is most likely due to the slow growth of CdTe nanocrystals at 100 °C.

2. Strong Nonmonotonic Difference in PL Efficiency of Size-Selected Fractions of CdSe, CdTe, and InAs Nanocrystals. Aliquots of the crude solutions of CdSe, CdTe, and InAs nanocrystals were taken at different stages of particle growth and divided into several (up to 12) fractions by carefully applying the size-selective precipitation technique. Figure 2 shows, as an example, the absorption and PL spectra of six size-selected fractions obtained from the crude solution of TOPO−TOP-capped CdSe nanocrystals. The size distribution in each fraction was, as expected, narrower than in the initial crude solution, leading to better pronounced electronic transitions in the absorption spectra and narrower PL bands (fwhm 30−35 nm). The absorption spectra of the size-selected fractions shifted to shorter wavelengths with decreasing mean particle size and were similar to those previously reported for monodisperse CdSe fractions.[1,4,20] Note, the efficiency of the band edge PL of all size-selected fractions of CdSe nanocrystals shows a clear dependence on the "fraction number". For instance, the first isolated fraction had lower PL efficiency than the other ones. The increase of the PL intensity from fraction to fraction was nonmonotonic: the maximum of the PL was observed in the present case for the fifth fraction with subsequent decrease for the sixth one. The difference between the lowest and the highest PL efficiencies was a factor of ∼3 (Figure 2).

Figure 3 shows that similar variations of the PL intensity are observed for size-selected fractions of the crude solution of CdSe nanocrystals with smaller average particle size. In all cases, the

(33) Kubin, R. F.; Fletcher, A. N. *J. Lumin.* **1982**, *27*, 455.
(34) Dawson, W. R.; Windsor, M. W. *J. Phys. Chem.* **1968**, *72*, 3251.

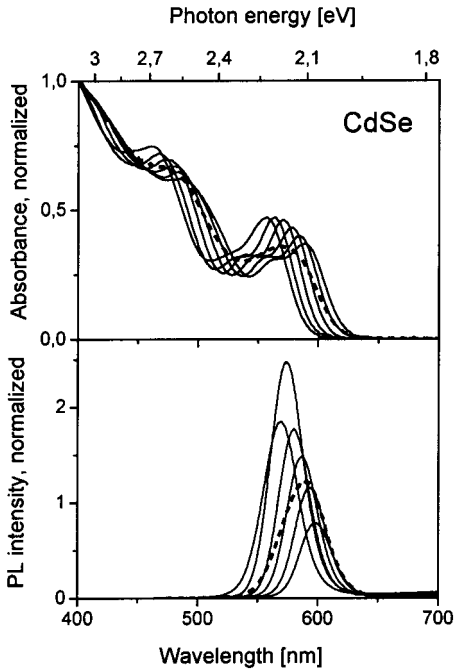

Figure 2. Absorption (top) and PL (bottom) spectra of size-selected fractions of CdSe nanocrystals (solid lines). The absorption and PL spectra of the crude solution (dashed lines) are added for comparison. PL intensities are normalized to identical absorbance at the excitation wavelength (400 nm).

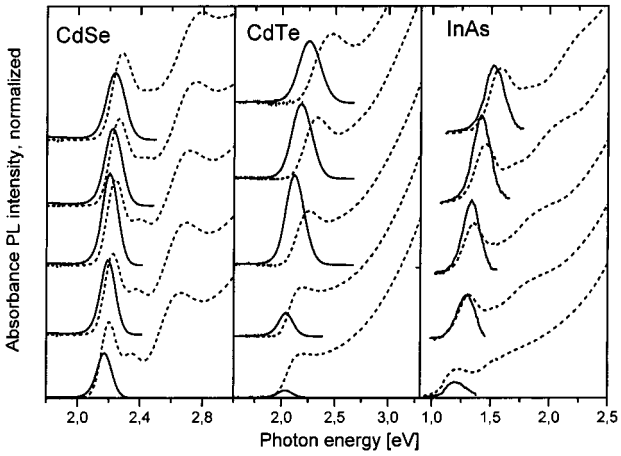

Figure 3. Absorption (dashed lines) and PL (solid lines) spectra of size-selected fractions of CdSe, CdTe, and InAs nanocrystals. For each material, all fractions were isolated from a single aliquot of the crude solution. All PL spectra were normalized with respect to the absorbed light intensity at excitation wavelength and plotted vs photon energy for better comparison of relative PL quantum efficiencies within each series of size-selected fractions.

fractions in the middle exhibit the highest PL efficiency. Size-selected fractions of TGA-stabilized CdTe nanocrystals and TOP-stabilized InAs nanocrystals showed the same PL dependence (Figure 3). Very similar behavior was also observed for the weak band edge emission of TOPO−TOP-capped InP nanocrystals (not shown). These results demonstrate that the phenomenon observed is common for colloids of different luminescent semiconductor materials.

The PL efficiencies observed for different fractions and materials are summarized in Figure 4. The points in this figure present both the absolute value of the PL efficiency (*Y*-axis) and the position of the PL maximum (*X*-axis) for each size-

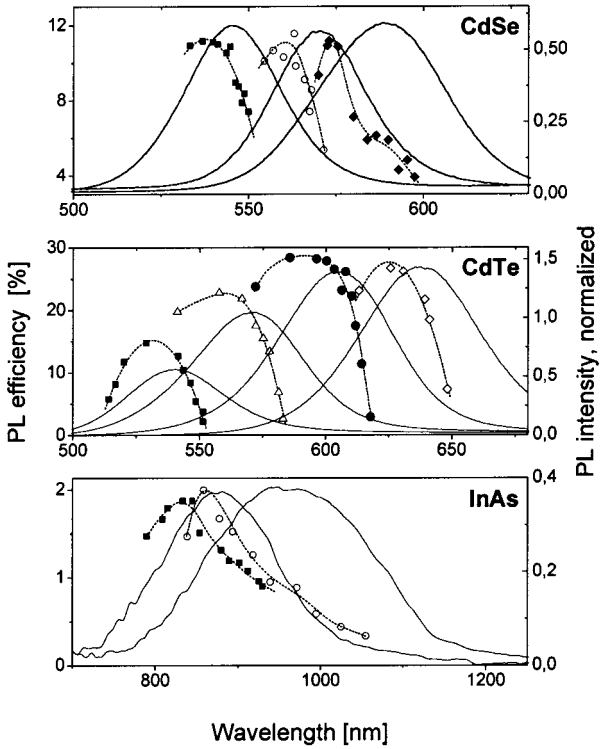

Figure 4. Solid lines: PL spectra of crude solutions of CdSe, CdTe, and InAs nanocrystals measured at different stages of particle growth. Points: PL quantum efficiency vs position of the PL maximum of size-selected fractions isolated from each crude solution.

selected fraction obtained from three (CdSe), four (CdTe), and two (InAs) crude solutions. The PL spectra of each crude solution are given as solid line; dashed lines present polynomial fits to the experimentally observed "PL efficiency−wavelength" dependencies in each series of fractions. For each series of either CdSe, CdTe, or InAs nanocrystals obtained through the size fractionation of the corresponding crude solutions, the PL efficiency−wavelength dependence clearly went through a maximum, which in all cases was shifted to shorter wavelengths in comparison to the position of the PL maximum of the corresponding crude solution. The PL efficiency varied systematically and very strongly within each series—up to 1 order of magnitude for CdTe nanocrystals (synthesized in aqueous solution and capped by thioglycolic acid) and up to ∼3−4 times for CdSe and InAs nanocrystals prepared organometallically.

Note that particles of the same size but obtained from crude solutions of different mean particle size exhibit different PL efficiencies (Figure 4). This means that the rather intriguing distribution of PL efficiencies observed within each ensemble of nanocrystals is not simply an effect of variation of PL efficiency with the particle size. [4,35]

To ensure that the PL behavior observed is not an effect of changes induced by the size-selective precipitation procedure (e.g., partial removal of stabilizing shell), we compared the initial crude solutions with solutions prepared by mixing all size-selectively isolated fractions in the same proportions as they were present in their crude solutions. In Figure 5a, the absorption and PL spectra of a crude solution of CdTe nanocrystals are compared with those of a corresponding remixed solution. Nearly quantitative agreement between the UV−visible and PL

(35) Qu, L.; Peng, Z. A.; Peng, X. *Nano Lett.* **2001**, *1*, 333.

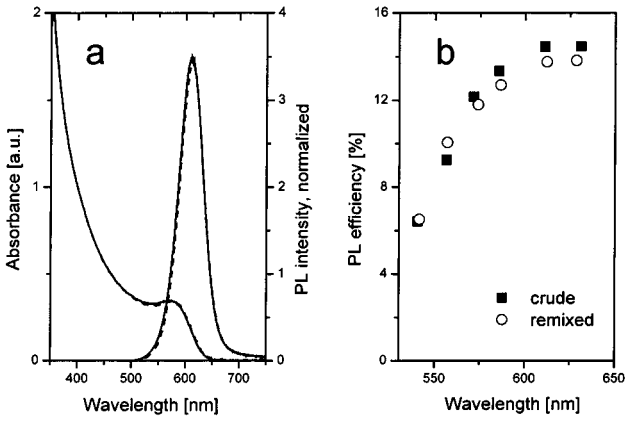

Figure 5. (a) Absorption and PL spectra of a crude solution of CdTe nanocrystals (solid line) and of a solution obtained by remixing all size-selected fractions isolated from this crude solution (dashed line). (b) PL quantum efficiency vs position of the PL maximum of crude solutions of CdTe nanocrystals measured at different stages of particle growth (■) and for the corresponding solutions prepared by remixing all size-selected fractions (○).

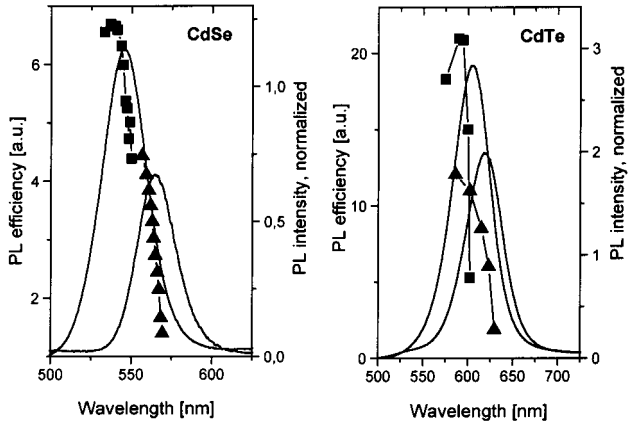

Figure 6. "PL quantum efficiency−wavelength" dependencies of size-selected fractions of CdSe and CdTe nanocrystals before (■) and after (▲) additional injection of precursors. The additional injections contained 60 (CdSe nanocrystals) and 35% (CdTe nanocrystals) of monomer compared to the amount initially employed.

spectra of the crude and the remixed solution was observed for all samples investigated. Minor differences in the PL maximums and the PL efficiencies (Figure 5b) obviously cannot be responsible for a 10-fold variation of the PL efficiency between size-selected fractions. This confirms that the size-selective precipitation and redissolution steps did not influence the PL properties of the nanocrystals.

Let us discuss the distribution of the PL efficiencies within an ensemble of nanocrystals grown in transient regime at early stages of the reaction, when the concentration of free monomer is high. The strong nonmonotonic difference in PL efficiency of size-selected fractions (Figure 4) was observed for rather late stages of the nanocrystal growth, when the Ostwald ripening growth mechanism accompanied by slow defocusing of the particle size distribution was probably achieved. In contrast, a high concentration of free monomer was present in the reaction mixture immediately after injection of precursors, and another regime of the nanocrystal growth accompanied with focusing of the particle size distribution was observed. However, investigation of the distribution of PL efficiencies immediately after start of the reaction was complicated due to the very small size of the nanocrystals at early reaction stages. The nanocrystals with size below ~2 nm usually have properties different from the larger ones. Thus, weak band edge PL, deep trap emission, "magic" particle sizes, stepwise growth of the nanocrystals from one "magic" size to another, etc., were reported for very small CdSe and CdTe nanocrystals.[1,31] Therefore, to obtain more correct results on the distribution of quantum efficiencies during particle growth at high concentration of free monomer (focusing of particle size distribution), we injected additional amounts of precursors into the crude solution of growing nanocrystals and measured the PL efficiency distribution within the ensemble before and after the injection. Addition of monomer to the reaction mixture caused rapid growth of the nanocrystals accompanied by focusing of their size distribution and a decrease of the PL intensity (Figure 6). Moreover, the "stationary" nonmonotonic PL efficiency distribution curve observed before the injection was disturbed after the additional injection, as shown in Figure 6 for CdSe and CdTe nanocrystals. Size-selected fractions obtained from the crude solutions of both, CdSe and CdTe nanocrystals, showed a monotonic dependence of the PL efficiency on the fraction number. The transition from stationary nonmonotonic toward monotonic dependence of the PL efficiency on the fraction number occurred quickly after the additional injection of precursors (within ~1 min for CdSe and ~10 min for CdTe nanocrystals) and did not change during early stages of defocusing of the particle size distribution. Thus, samples of CdSe and CdTe nanocrystals taken in 40 min and 2 h after additional injection, correspondingly, still exhibited monotonic variation of PL efficiency from fraction to fraction. In case of CdTe nanocrystals, long-term (~10 h) heating resulted in recovery of the nonmonotonic distribution of PL efficiency within the ensemble of nanocrystals. In case of CdSe nanocrystals, the PL efficiency after additional injection continuously decreased in time and became nearly zero after several hours of particle growth at 300 °C, so that no reliably data concerning recovery of "stationary" PL efficiency distribution were obtained in this case.

3. Comparison of the Nanocrystal Fractions with the Lowest and the Highest PL Efficiency. In the second series of experiments, we compared the properties of size-selected nanocrystals belonging to the fraction with the lowest PL efficiency (below referred to as LPL fraction) with those belonging to the fraction showing the highest PL efficiency (HPL fraction).

A direct comparison of HRTEM images of CdSe, CdTe, and InAs nanocrystals did not reveal any statistically reliable difference between particles of the HPL and the LPL fractions with respect to average particle crystallinities, shapes, lattice distances, etc. Thus, in the case of CdSe nanocrystals possessing hexagonal (wurtzite) lattice, both the LPL and the HPL fractions consisted of very similar nearly spherical particles (see the images in Supporting Information), so that the difference between LPL and HPL fractions cannot be explained by a difference in the particle shape. The low contrast of the presurface lattice planes in the HRTEM images did not allow any comparison of the surface roughness of nanocrystals. No systematic difference between LPL and HPL fractions was observed in the powder XRD patterns as well. Thus, both methods of direct probing the nanocrystal lattices—HRTEM and

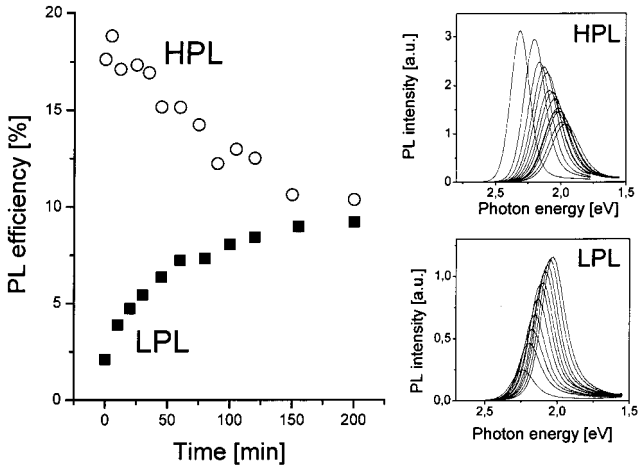

Figure 7. Left: temporal evolution of the PL quantum efficiency of two different size-selected fractions of CdTe nanocrystals upon growth in a solution with composition similar to the crude solution. LPL is the size-selected fraction with the lowest PL quantum efficiency; HPL is the fraction with the highest PL quantum efficiency. Right: change of the PL spectra of the LPL and HPL fractions during further growth.

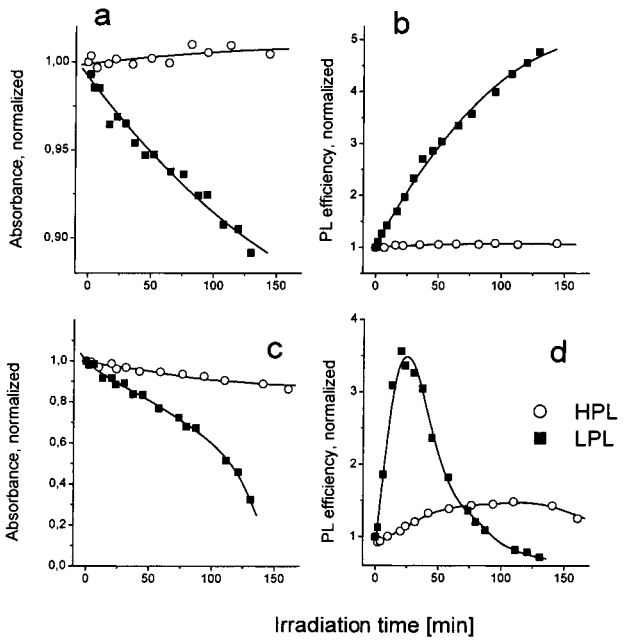

Figure 8. Difference in photostability of the LPL (■) and the HPL (○) fractions of CdTe nanocrystals under irradiation with 400-nm light of a 450-W xenon lamp. (a) and (c) show the temporal evolution of the absorption at 400 nm; (b) and (d) show the evolution of the PL quantum efficiency vs irradiation time. Both absorption and PL quantum efficiency are normalized to their initial values (i.e., before irradiation). (a) and (b) were measured under argon; (c) and (d) were measured in oxygen-saturated solutions.

powder XRD—demonstrated that both LPL and HPL fractions were very similar with respect to the particle crystallinitiy and shape.

The different behavior of LPL and HPL fractions of size-selected nanocrystals will be further demonstrated in this paper on TGA-capped CdTe nanocrystals as they showed the largest difference in the PL efficiencies and were better processable as compared to CdSe and InAs nanocrystals. In the latter cases, all manipulations had to be performed inside the glovebox to achieve reproducible results. However, the behavior described below was general and was observed for CdSe and InAs nanocrystals as well.

Figure 7 shows the evolution of the PL intensity during further growth of CdTe nanocrystals from the LPL and HPL fractions. Size-selected nanocrystals were placed in solutions of the same composition (i.e., the same concentrations of the nanocrystals, stabilizer, cadmium ions and the same pH) as the initial crude solution the fractions were isolated from, and growth of the nanocrystals was initiated by refluxing. After some time, both samples reached approximately the same size. After growth, both, the LPL fraction and the HPL fraction, showed nearly the same PL efficiencies: they returned to a mean value of ~9%, i.e., the same value as in the initial crude solution of the nanocrystals (PL efficiency 10 ± 2%). After size-selective fractionation, the "PL efficiency − fraction number" dependence of these solutions was almost identical to that observed for the initial crude solution.

Further, the LPL and HPL fractions of CdTe nanocrystals evolved very differently under UV-light irradiation (Figure 8). Both in argon- and in air-saturated solutions, the nanocrystals from the HPL fraction were remarkably more photostable (Figure 8a and c, respectively) as evidenced from the temporal evolution of the absorption spectra. We also observed an improvement of the PL efficiencies of both the LPL and HPL fractions at the initial stage of irradiation, which was much more pronounced for the LPL fraction (Figure 8b, d).

Discussion

As was shown in the Results section, the PL efficiency varies strongly within any ensemble of as-prepared semiconductor nanocrystals (Figures 2 and 3). We observed similar behavior for nanocrystal ensembles prepared via different synthetic routes (Figure 4). The fact that the PL efficiency distribution keeps nearly constant during particle growth in the Ostwald ripening regime suggests that the growth mechanism itself might be the cause for this distribution of properties within each ensemble.

To clarify possible origins of this variation, we compared the properties of the fractions with the lowest and the highest PL efficiencies. No distinct difference between LPL and HPL fractions was found by XRD and HRTEM studies. On the other hand, if these size-selected fractions of nanocrystals were allowed to grow further at conditions of Ostwald ripening, their size distribution and PL efficiency developed toward values typical for the crude solution from which the fractions were isolated (Figure 7).

The higher photostability of the nanocrystals of the HPL fraction (Figure 8a,c) indicates that their surface quality is much better in terms of a smaller number of surface defects serving as centers of photooxidation. In fact, an enhancement of the PL efficiency under irradiation similar to that found for the LPL fraction (Figure 8b,d) was observed for several kinds of nanocrystals[36,37] and was attributed to processes resulting in the annealing of surface defects acting as traps for photogenerated carriers.[36] Annealing under irradiation should be more pronounced for nanocrystals with a higher concentration of defects at the particle surface (i.e., for the LPL fraction). Thus, summarizing the behavior observed for the LPL and HPL fractions, we can suggest that the difference between their PL efficiencies originates from the different surface quality (or

(36) Resch, U.; Weller, H.; Heinlein, A. *Langmuir* **1989**, *5*, 1015.
(37) Gerion, D.; Pinaud, F.; Williams, S. C.; Parak, W. J.; Zanchet, D.; Weiss, S.; Alivisatos, A. P. *J. Phys. Chem. B* **2001**, *105*, 8861.

surface disorder) of nanocrystals—in this paper, we use this general term to describe a smooth and defect-free surface (to a smaller or larger extent) being free of traps. The difference in the surface quality of nanocrystals in an ensemble originates from the growth conditions and is not caused by the size-selective precipitation after preparation. The latter is only a tool to isolate fractions of nanocrystals with different surface quality and size.

Why does the surface quality vary in an ensemble of growing nanocrystals systematically with the nanocrystal size? To answer this question we have to consider the parameters governing the surface quality or surface roughness of crystalline solids during their growth. The surface roughness of bulk crystals depends strongly on the growth conditions, mainly on the ratio between the growth temperature and the characteristic temperature (T_R) of the so-called "roughening transition".[38−41] Below T_R, the surface of the growing crystal is microscopically smooth, above it is rough. For most semiconductors, T_R is above 1000 °C, being slightly dependent on the crystallographic plane.[39] In principle, for nanocrystalline matter, T_R can be much lower, as the melting point depends on the particle size.[42] However, even if we assume that T_R is size-dependent, it would not allow us to explain similar distributions of surface quality within ensembles with different mean particle size. Therefore, it seems more probably that the observed distribution of PL efficiencies can be explained in terms of "kinetic roughening", the phenomenon well known for the growth of bulk crystalline solids:[38,43,44] when growth rate of a crystal increases, the critical size of two-dimensional (2D) nucleation sites at the surface becomes so small that the 2D nucleation barrier vanishes. As a result, the crystal surface becomes microscopically rough and macroscopically rounded.

In an ensemble of nanocrystals in colloidal solution, the particle growth rate is strongly size-dependent: the main concept of the Ostwald ripening implies that larger particles in an ensemble grow at the expense of monomer released by the dissolution of smaller particles. As the Ostwald ripening is a self-similar process with an unique limiting particle size distribution,[45−55] the particle growth rate distribution has to be similar at all stages of the particle growth. To explain the influence of the growth mechanism on the distribution of PL efficiency in any ensemble of growing colloidal nanoparticles, we developed a model describing the evolution of a nanocrystal ensemble growing in a solution of monomer.

Theoretical Description of the Dynamic Growth Rate Distribution within the Ensemble of Nanocrystals. To describe the evolution of an ensemble of nanoparticles in colloidal solution, several processes occurring simultaneously have to be considered: the kinetics of the addition or the removal of monomer from the nanocrystals, changes of the particle concentration with time due to nucleation and dissolution processes, temporal evolution of the monomer concentration, etc. A theory of Lifshitz, Slyozov, and Wagner (LSW)[45,46] provides an asymptotic solution for the evolution of an ensemble of particles during Ostwald ripening. However, this approach as well as further analytical models and numerical simulations of Ostwald ripening[47−55] fails in the description of ensembles of nanometer-sized particles as only two terms of the expansion of the Gibbs−Thompson equation are used:

$$C(r) = C^0_{\text{flat}} \exp\left[\frac{2\gamma V_m}{rRT}\right] \approx C^0_{\text{flat}}\left(1 + \frac{2\gamma V_m}{rRt}\right) \qquad (1)$$

where C(r) and C^0_{flat} are the solubilities of a particle with radius r and of the bulk material, respectively, γ is the surface tension, and V_m is the molar volume of the solid.

The coefficient $2\gamma V_m/(RT)$ called "capillary length" is usually of the order of 1 nm,[51,52] and eq 1 satisfactorily describes the solubility of colloidal particles with radius larger than ~20 nm. For nanocrystals with $r = 1-5$ nm, the value of the capillary length is approaching the particle radius, and the particle solubility becomes strongly nonlinear against r^{-1}. On the other hand, the Gibbs−Thompson equation in its exact form is, probably, valid for very small particles: it was reported that the surface tension remains nearly constant for many interfaces even if the particle size is as small as ~1 nm.[56]

Recently, we proposed a model of particle growth and dissolution which is based on the dependence of activation energies on the particle size.[23] This model allows us to describe the size-dependent evolution of a nanoparticle under reaction, diffusion, and mixed reaction−diffusion control. Thus, the evolution of a single particle of radius r in a solution of monomer with constant concentration [M] is given by the following equation (see details in ref 23):

$$\frac{dr^*}{d\tau} = \frac{S - \exp[1/r^*]}{r^* + K\exp[\alpha/r^*]} \qquad (2)$$

where $r^* = (RT/2\gamma V_m)r$ and $\tau = (R^2T^2DC^0_{\text{flat}}/4\gamma^2V_m)t$ are dimensionless particle radius and time, respectively. $K = (RT/2\gamma V_m)(D/k_g^{\text{flat}})$ is the dimensionless parameter describing the type of the process involved, i.e., the ratio between the rates of a purely diffusion-controlled process (D is the diffusion coefficient of the monomer) and a purely reaction-controlled one (k_g^{flat} is a first-order reaction rate constant for the process of addition of a monomer to a flat interface; see ref 23 for details). Thus, a value of $K < 0.01$ corresponds to the almost pure diffusion-controlled process, $K > 100$ corresponds to the reaction-controlled one, and the range $0.01 < K < 100$ corresponds to the regime of mixed control with comparable contributions of both processes.

The dimensionless parameter $S = [M]_{\text{bulk}}/C^0_{\text{flat}}$ describes the oversaturation of the monomer in solution; α is the transfer coefficient of the activated complex ($0 < \alpha < 1$).

(38) Liu, X. Y.; Bennema, P. *J. Cryst. Growth* **1994**, *139*, 179.
(39) Heyraud, J. C.; Métois, J. J.; Bermond, J. M. *Surf. Sci.* **1999**, *425*, 48.
(40) Jackson, K. A.; Miller, C. E. *J. Cryst. Growth* **1977**, *40*, 169.
(41) Vakarin, E. V.; Badiali, J. P. *Phys. Rev. B* **1999**, *60*, 2064.
(42) Goldstein, A. N.; Echer, C. M.; Alivisatos, A. P. *Science* **1992**, *256*, 1425.
(43) Scneidman, V. A.; Jackson, K. A.; Beatty, K. M. *J. Cryst. Growth* **2000**, *212*, 564.
(44) Gilmer, G. H. *J. Cryst. Growth* **1976**, *35*, 15.
(45) Lifshitz, I. M.; Slyozov, V. V. *J. Phys. Chem. Solids* **1961**, *19*, 35.
(46) Wagner, C. *Z. Elektrochem*. **1961**, *65*, 581.
(47) Marqusee, J.; Ross, J. *J. Chem. Phys.* **1984**, *80*, 536.
(48) Voorhees, P. W. *J. Stat. Phys.* **1985**, *38*, 231.
(49) Yao, J. H.; Elder, K. R.; Guo Hong; Grant, M. *Phys. Rev. B* **1993**, *47*, 14110.
(50) Venzl, G. *Phys. Rev. A* **1985**, 31, 3431.
(51) Kabalnov, A. S.; Shchukin, E. D. *Adv. Colloid Interface Sci.* **1992**, 38, 69.
(52) De Smet, Y.; Deriemaeker, L.; Finsy, R. *Langmuir* **1997**, *13*, 6884.
(53) Carlow, G. R.; Zinke-Allmang, M. *Phys. Rev. Lett.* **1997**, *78*, 4601.
(54) De Smet, Y.; Deriemaeker, L.; Parloo, E.; Finsy, R. *Langmuir* **1999**, *15*, 2327.
(55) Egelhaaf, S.; Olsson, U.; Schurtenberger, P.; Morris, J.; Wennerström, H. *Phys. Rev. E* **1999**, *60*, 5681.
(56) Fenelonov, V. B.; Kodenyov, G. G.; Kostrovsky, V. G. *J. Phys. Chem. B* **2001**, *105*, 1050.

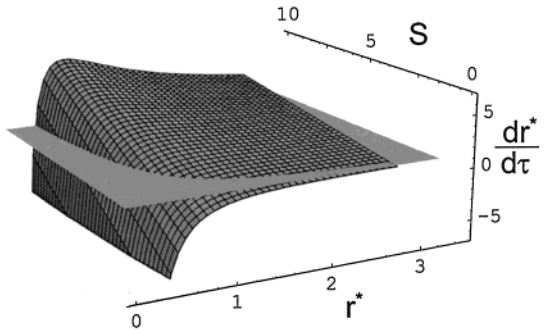

Figure 9. Growth rate vs nanocrystal radius for different values of the monomer oversaturation *S* as calculated from eq 2 for a single nanocrystal under diffusion control ($K = 0.01$). The gray plane corresponds to zero growth rate of the nanocrystal.

The growth rate of a single nanocrystal depends strongly on its radius and on the concentration of monomer in solution close to the nanocrystal surface. The size dependencies of the nanocrystal growth rate were calculated from eq 2 for different values of *S* and are presented in Figure 9. Note that nanocrystals smaller than a critical radius r_{ZGR} have negative growth rates; i.e., they dissolve. The critical radius corresponding to a net growth rate equal to zero ($dr^*/d\tau = 0$) can be easily derived from eq 2:

$$r_{ZGR} = 2\gamma V_m/(RT \ln S) \quad (3)$$

where the index ZGR indicates "zero growth rate".

The zero growth rate in terms of a real ensemble of growing nanocrystals implies that the average rate of removal of matter from the nanocrystals is equal to the rate of addition of monomer to the nanocrystal surface. In a real experiment, a large number of colloidal particles compete for a finite amount of monomer and the monomer is consumed during nanocrystal growth. As a result, the bulk concentration of monomer and the oversaturation *S* decrease gradually. This results in a shift of r_{ZGR} toward larger sizes and a decrease of the nanocrystal growth rate (Figure 9).

A general analytical solution describing all processes occurring during the evolution of the entire ensemble could not be obtained. For this reason, the Monte Carlo simulation technique was applied to obtain statistical information about the ensemble behavior. Monte Carlo modeling of the nanocrystal ensemble was rather straightforward, and the principle was identical to that reported in refs 23 and 52. The evolution of each nanocrystal was described by eq 2. The value of the monomer oversaturation *S* in the solution was calculated after each time step from the conservation law for the monomer and was substituted into eq 2 to recalculate new rates of growth/dissolution of nanocrystals. The numerical parameters used in the simulation procedure (see Supporting Information) were chosen to be in reasonable agreement with experimental conditions.[20,32] We assumed complete separation of nanocrystal nucleation and growth (e.g., by the hot injection technique). This implies that an ensemble of nanocrystal nuclei with a given size distribution had formed before particles start to grow. As was predicted by LSW theory and confirmed by our numerical simulations, the parameters of the initial size distribution of nuclei do not affect the later stages of particle growth. After a short transient time, the ensemble evolves toward a unique particle size distribution independent of the initial conditions.

In accord with the mechanism of Ostwald ripening, the largest particles in the ensemble have positive and the smallest have negative growth rates (Figure 9). Between these two cases there are particles having nearly zero net growth rate. In other words, at any given instant of time, the oversaturation of the monomer is different for different nanocrystals in the ensemble and equal to zero for nanocrystals with a size corresponding to ZGR.

The main goal of the simulations performed was to establish the intrinsic distribution of the particle growth rates within the ensemble at different stages of its evolution. Figure 10a presents the temporal evolution of the nanocrystal size distribution during diffusion-controlled Ostwald ripening (K=0.001). It is clearly seen that the initially symmetric normal particle radius distribution evolves in time toward an asymmetric negatively skived one. Figure 10b shows a particle size distribution curve of the nanocrystal ensemble grown from a mean particle radius of 1.0 to 3.5 nm. The dashed line gives the size dependence of the single-particle growth rate as calculated from eq 2 for the current value of oversaturation. The particle size corresponding to ZGR is marked by an arrow and is shifted from the maximum of the particle size distribution toward smaller particles. Coming back to Figure 10a, one can see that particles with ZGR are situated at the left part of the entire ensemble at all stages of growth.

The monomer preferably leaves the nanocrystals from surface sites having the highest energy (defects, kinks, etc.). On the other hand, monomers tend to join the most energetically favorable positions at the surface. The kinetic roughening approach evidences that the most ideal conditions for annealing of surface defects are realized at small growth rate of the crystal. Consequently, particles with a size close to r_{ZGR} do possess the most smooth and defect-free surfaces of all particles in the ensemble. In fact, comparison of the data presented in Figures 2 and 4 with results of numerical simulations (Figure 10) demonstrates that size of the particle with the highest PL efficiency (HPL fraction) within the ensemble coincides well with the ZGR size.

According to the simulation, instantaneous increase of the oversaturation of monomer (e.g., by additional injection of precursors) shifts r_{ZGR} to very small values located outside the particle size distribution (Figure 10c). As a result, all nanocrystals possess positive growth rates and the growth rate increases monotonically with the particle size. The higher particle growth rates should result in larger surface roughness and, as a consequence, in a larger concentration of surface defects and lower PL efficiency.[25,43] In agreement with these predictions, a monotonic decrease of the PL efficiency with increasing particle size (decreasing fraction number) was observed for size-selected fractions of CdSe and CdTe nanocrystals after additional injection of precursors (Figure 6).

Outlook for Material Science Applications

The findings of this work are important for the use of highly luminescent nanocrystals in optoelectronic, photonic, and tagging applications. Thus, the simple postpreparative size-selective precipitation of the CdTe nanocrystals described above provides water-soluble, stable, highly processable, and surface-functionalized (as almost any type of short-chain thiols can be used as stabilizer) particles with PL efficiencies of up to 20−30%. This value can be enhanced further: as was shown in ref 32, the PL efficiency of TGA-capped CdTe nanocrystals can be consider-

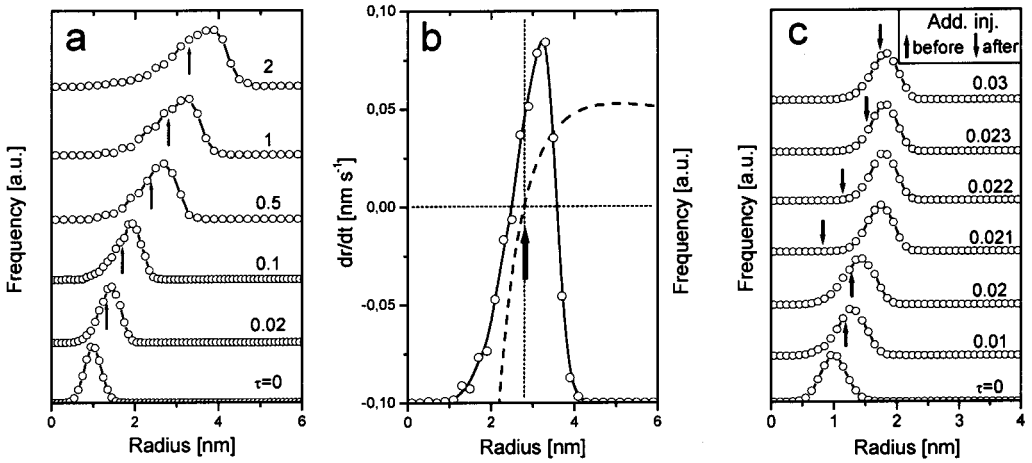

Figure 10. (a) Monte Carlo simulations of the temporal evolution of an ensemble of nanocrystals during Ostwald ripening under diffusion control ($K = 0.001$). Arrows indicate the particle size for which the average particle growth rate is zero (ZGR). (b) Solid line and open circles: "stationary" particle size distribution after prolonged growth of an ensemble of nanoparticles: shape of the distribution becomes independent of time. Dashed line: growth rate vs particle size for a single nanoparticle. The arrow shows the particle size with zero average growth rate. (c) Monte Carlo simulations of the particle size with zero growth rate (shown by arrows) within an ensemble of growing nanocrystals before and after additional injection of monomer (80% of the initial amount added) at $\tau = 0.02$. Nanocrystals grow via diffusion-controlled Ostwald ripening ($K = 0.001$, $S_0 = 15$).

ably increased by forming a shell of cadmium thiolate complexes at the surface of nanoparticles. The PL quantum efficiency of CdTe nanocrystals from the HPL fraction reached a value of 47% after this treatment.

Moreover, we found that CdSe/ZnS and InAs/CdSe core/shell nanocrystals prepared from the HPL fractions of CdSe and InAs cores exhibited really superior luminescent properties. Probably, the smooth surface of nanocrystals of the HPL fraction results in a better passivation of the nanocrystals by the epitaxial layer of the wide band-gap semiconductor. This is also in accord with a common statement that the best core/shell nanocrystals can be prepared from cores with highest PL efficiencies.

The use of HPL fractions for the preparation of core/shell nanocrystals seems to be a general way to further improve the properties (PL efficiency, stability, etc.) of luminescent nanocrystals.

Summary

We have found a drastic difference in the PL efficiency of size-selected fractions of CdSe, CdTe, and InAs nanocrystals. We suggest that the difference in the PL efficiency originates from the variation of the surface quality within an ensemble of growing nanocrystals. High surface quality in this paper refers to a smooth, defect-free, and thus a charge carrier trap-free surface. On the basis of a theoretical model describing the evolution of an ensemble of nanocrystals growing in a solution of monomer, we propose that the nanocrystal fraction with the best surface quality and, thus, with the most efficient PL corresponds to the particle size with the smallest net growth rate within the ensemble. Since annealing of surface defects is most effective at this "zero growth rate", this condition leads to the highest possible surface quality.

Independent of the kind of nanocrystals, it is definitely worth looking for the fraction with the highest PL efficiency of a given ensemble if further use of the nanocrystals requires high luminescence efficiency. In any case, coming from an averaged ensemble behavior to any application based on the single-particle response (e.g., biolabeling,[17−19] single-particle fluorescence,[26] transistor based on a single nanocrystal[16]), the intrinsic difference between nanocrystals within an ensemble starts to play a dominant role and must be taken into account.

Acknowledgment. We thank Dr. S. Haubold (Nanosolutions GmbH, Hamburg) and Dr. N. P. Gaponik for help in preparation of InAs and CdTe nanocrystals, and Dr. A. Eychmüller for stimulating discussions. We also thank J. Kolny and J. Ludwig for the powder XRD measurements. This work was supported in part by the research project BMBF-Philips and Deutsche Forschungsgemeinschaft (SFB 508).

Supporting Information Available: HRTEM images and powder XRD patterns of CdSe, CdTe, and InAs nanocrystals; the numerical parameters used in the Monte Carlo simulation procedure. This material is available free of charge via the Internet at http://pubs.acs.org. See any current masthead page for ordering information and Web access instructions.

JA0123599